Geomechanics and Engineering, *Vol. 30, No. 6 (2022) 539-549*
https://doi.org/10.12989/gae.2022.30.6.539

Centrifuge modeling of dynamically penetrating anchors in sand and clay

Xiaoyu An[1,2], Fei Wang[2], Chao Liang*[1] and Run Liu[1]

[1]*State Key Laboratory of Hydraulic Engineering Simulation and Safety, Tianjin University, Tianjin 300072, China*
[2]*National Engineering Laboratory for Port Hydraulic Construction Technology, Tianjin Research Institute for Water Transport Engineering, M.O.T., Tianjin 300456, China*

(*Received June 24, 2022, Revised August 25, 2022, Accepted August 30, 2022*)

Abstract. Accidental anchor drop can cause disturbances to seabed materials and pose significant threats to the safety and serviceability of submarine structures such as pipelines. In this study, a series of anchor drop tests was carried out to investigate the penetration mechanism of a Hall anchor in sand and clay. A special anchor drop apparatus was designed to model the in-flight drop of a Hall anchor. Results indicate that Coriolis acceleration was the primary cause of large horizontal offsets in sand, and earth gravity had negligible impact on the lateral movement of dropped anchors. The indued final horizontal offset was shown to increase with the elevated drop height of an anchor, and the existence of water can slow down the landing velocity of an anchor. It is also observed that water conditions had a significant effect on the influence zone caused by anchors. The vertical influence depth was over 5 m, and the influence radius was more than 3 m if the anchor had a drop height of 25 m in dry sand. In comparison, the vertical influence depth and radius reduced to less than 3 m and 2 m, respectively, when the anchor was released from 10 m height and fell into the seabed with a water depth of 15 m. It is also found that the dynamically penetrating anchors could significantly influence the earth pressure in clay. There is a non-linear increase in the measured penetration depth with kinematic energy, and the resulted maximum earth pressure increased dramatically with an increase in kinematic energy. Results from centrifuge model tests in this study provide useful insights into the penetration mechanism of a dropped anchor, which provides valuable data for design and planning of future submarine structures.

Keywords: anchor drop test; centrifuge modeling; earth pressure; kinematic energy; penetration mechanism

1. Introduction

Since China joined the World Trade Organization (WTO) in 2001, there has been an ever-increasing amount of cargo transportation and commodity flow using marine transport due to its relatively cheap transport cost. To cope with the challenging demand, there is a concurrent increase in the ship tonnage for ports and berths along both coastal and inland waterways in China. In order to fasten a giant ship to the seabed, anchors of larger sizes and self-weight are adopted, which are more susceptible to incidents (Nakamura *et al.* 2002). Previous research reveals that most of those incidents are caused by accidental anchor drop and a dropped anchor can penetrate into the seabed and cause significant disturbances to submarine pipelines, which are laid on the seabed or with a shallow embedment (Gao *et al.* 2018, Tian *et al.* 2021). Therefore, it is imperative to have a sound understanding of anchor penetration mechanisms before design and analysis of submarine structures such as pipelines.

Currently, there are quite limited studies regarding the penetration mechanism of a dropped anchor. True (1975) developed analytical solutions to investigate the penetration behavior of projectiles into seafloor materials. Note that the method only applies to sharp projectiles with large initial velocity, which is quite different from the behavior of a conventional ship anchor. It is also challenging to simulate the dynamically penetrating process of a dropped anchor using advanced numerical methods. Some scholars have also carried out relevant research. Wang *et al.* (2009) used 3-D non-linear numerical analysis code ABAQUS/Explicit to simulate the entire process from the anchor being dropped into the seabed to the anchor being dragged out of the seabed and through the rock protection cover. Ouyang *et al.* (2016) used non-linear finite element program (LS-DYNA/ANSYS) to established a geometric model of anchor, seabed and pipeline to restore the process of the anchor penetrating in the seabed, and analyzed the dynamic response process of contact and collision between the anchor and seabed. Zhu *et al.* (2019) formulated a calculation method for the bottoming speed of an anchor, the depth of anchor penetration was calculated. On the basis of the findings, the calculation results were further analyzed, and conclusions were derived regarding the relationship between anchor mass, the horizontal projected area of the anchor, the anchor height on the water surface, and water depth. Numerical simulation models of submarine pipelines are established by Zhang *et al.* (2020) to investigate the damage mechanisms, mechanical behaviors, and energy absorptions of submarine pipelines impacted by bar-shaped objects based on multiple theories and approaches. The effects of essential physical parameters on the impact behaviors of submarine pipelines are discussed.

Many studies carried out physical model tests (Shin *et*

*Corresponding author, Ph.D.
E-mail: liangchao@tju.edu.cn

ISSN: 2005-307X (Print), 2092-6219 (Online)

Table 1 Relevant scaling laws

Parameter	prototype ratio	Parameter	prototype ratio
	1/n	Acceleration	n
Area	1/n^2	Force	1/n^2
Volume	1/n^3	Stress	1
Mass	1/n^3	Strain	1
Density	1	Displacement	1/n
Time	1/n		

al. 2011, Han *et al.* 2019), either 1 g physical modeling using either reduced-scale or full-scale anchors, which are considered the most commonly adopted method to investigate penetration behaviors of dropped anchors. A series of anchor drop tests were conducted by Liu *et al.* (2020) to analyze the influence of anchor mass and drop height on the penetration depth of hall anchor and high holding power anchor in cohesive and non-cohesive soils. Wang *et al.* (2016) conducted 128 sets of penetration experiments with nine model anchors. A formula calculating the penetration depth in soft wet soil is proposed. The speed of the anchor was obtained by experimental method when the anchor falling to the seabed above the pipeline (Hu *et al.* 2021). Meanwhile, the maximum impact force of the dropping anchor at different protective layer situation was also tested. Note that 1g physical model tests cannot correctly model in-situ soil stresses and, the obtained results are qualitative and can be problematic if directly applied to solve real applications (Taylor *et al.* 1995, Madabhushi *et al.* 2015). In comparison, full-scale tests can provide useful insights into the governing penetration mechanism but may involve large costs and human resources.

The above-mentioned challenges can be effectively addressed using centrifuge modelling, which enables the accurate replication of in-situ soil stresses around a reduced-scale model based on appropriate scaling relationships (Cho *et al.* 2018, Wang *et al.* 2018). It is also convenient to change soil and anchor types, anchor drop height and water conditions for parametric analyses.

In this study, a series of centrifuge model anchor drop tests was carried out to investigate penetration mechanisms of anchors in sand and clay. A special designed apparatus was developed for in-flight drop of Hall anchors. The test results provide useful insights into the influence zone and earth pressure change of soils subjected to a dropped anchor, and provide valuable data for design and analysis of submarine structures such as pipelines.

2. Experimental design and workflow

The principle of geotechnical centrifuge modeling is to recreate in-situ soil stresses using a reduced model scale but at an enhanced centrifugal acceleration. Assume that a model uses the same material as the prototype but with a reduced dimension (i.e., prototype/model=n). When the centrifugal acceleration rises to ng, the in-situ stress (=γ×1/n×ng=γ×g) is identical for both the reduced-scale model and full-scale prototype (Ng *et al*. 2013b, Fang *et al.* 2022, Shi *et al*. 2022a, Shi *et al*. 2022b). Table 1 summarizes the key scaling relationships between model and prototype.

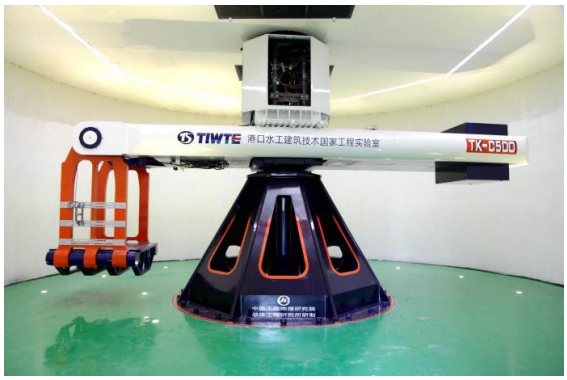

Fig. 1 TK-500 geotechnical centrifuge

Table 2 Test program

Test No.	Soil type	Anchor weight (ton)	Drop height (m)	Water level above seabed(m)
1	Dry sand	2.26	10	N/A
2			12.5	
3			15	
4			17.5	
5			20	
6			22.5	
7			25	
8	Saturated sand		10	5
9			10	10
10			10	15
11	Saturated clay	6	2.0	N/A
12			4.2	
13			7.5	
14		12.3	1.9	
15			4.2	
16			7.5	
17		23.4	0.6	
18			2.1	
19			4.6	
20			7.3	

*The values represent vertical distance above the water level.

2.1 Experimental program

All the centrifuge model tests were carried out at geotechnical engineering research center of Tianjin research institute for water transport engineering. Fig. 1 shows an overview of the TK-C500 centrifuge which has a maximal modelling capacity of 250 g·t. The swing platform has a dimension of 1.4 m×1.5 m×1.5 m.

Table 2 summarizes the experimental test program. In total, twenty centrifuge model tests, i.e., ten in sand and ten in clay, were conducted. Of all the mode tests in sand, seven tests were performed in dry sand with various drop heights ranging between 200 mm (10 m in prototype) and 500 mm (25 m in prototype) in order to obtain various landing velocities. The remaining three tests were carried out in saturated sand with a water level of between 100 mm (5 m

Table 3 Dimensions of 2.28 ton A-type Hall anchor

Symbol	Value (mm)
$H+H_1+h_1$	2745
h	1165
L_1	1165
L	1657
B	645
α	42

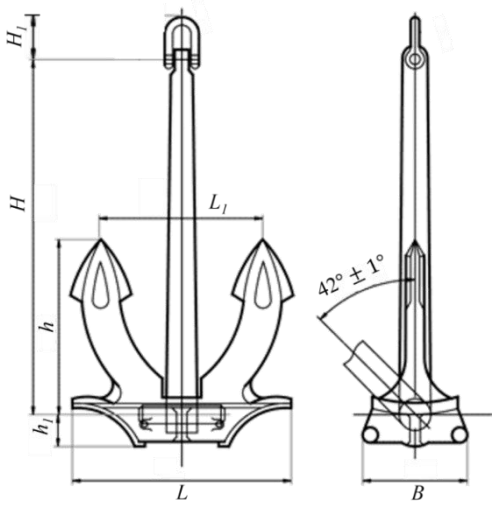

Fig. 2 Schematic diagram of 2.28 ton A-type Hall anchor

in prototype) and 300 mm (15 m in prototype) above the sand bed. However, the free-fall height of the anchor was fixed at 200 mm (10 m in prototype) above the water level before release during in-flight testing. The drop height was chosen to represent a worst design scenario according to Chinese ship design manual. In addition, each model test was repeated three times to ensure accuracy and robustness. The test acceleration is 50 g.

Apart from above-mentioned model tests in sand, ten anchor drop tests were also carried out in saturated clay. The test acceleration is 70 g. More specifically, anchors with three different prototype weights (i.e., 6 ton, 12.3 ton and 23.4 ton) were adopted. Each anchor was designed to release from three prototype heights, i.e., 2.1 m, 4.2 m and 7 m. Due to differences in model preparation, the actual measured drop height was slightly different from the designed height. It is also worth pointing out that the ground water level was the same as the levelled surface of the clay. Note that the existence of water may reduce the impact force of a dropped anchor. Therefore, the model tests in clay essentially simulate a worse design scenario. In fact, the maximum impact force imposed by a dropped anchor can be represented in terms of total kinematic energy ($1/2\ mv^2$), which is a product of a coefficient (0.5), mass (m) and the square of landing velocity (v). For example, the maximum kinematic energy for a 23.4 ton prototype anchor is 1664.6 kJ at a drop height of 7.3 m.

2.2 Model ship anchor and instrumentation

Apart from modelling in-situ soil stresses, geometries and self-weight of an anchor should also be properly replicated in centrifuge model tests in order to accurately evaluate the penetration mechanism of an anchor. In practical engineering applications, the adopted type and size of an anchor should be determined according to the sailing and water conditions along the shipping route. In this study, a 2.28 ton "A" type hall anchor was adopted for testing in sand, as shown in Fig. 2. Table 3 shows the prototype dimensions of the selected A-type hall anchor (GB/T 546-2016).

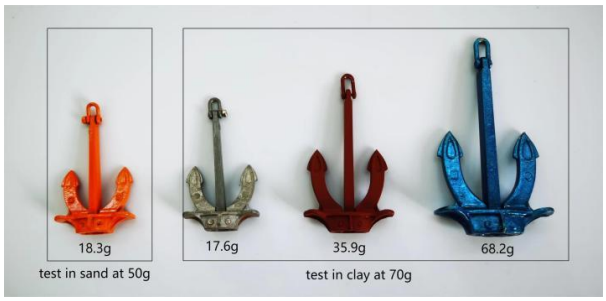

Fig. 3 A typical 3D printed model anchor

The hall anchor has relatively complex geometries, and it is challenging to make a model anchor using traditional methods such as welding from individual metal plates. In this study, the model hall anchor was directly 3D printed using stainless steel. Fig. 3 shows all the model anchor.

The model weight of 18.3 gram (equivalent to 2.28 ton in prototype at 50 g) was printed for the sand test, and the other three anchors with model weights of 17.6, 35.9 and 68.2 gram (equivalent to 6, 12.3 and 23.4 ton at 70 g) were printed for testing in clay.

In order to measure the earth pressure variation and associated influence zone resulted from a dropped anchor, multiple earth pressure sensors were embedded in sand at various depths. Fig. 4(a) shows the instrumentation and monitoring setup for model tests in sand. In total, eight were installed in each of the ten model tests in sand. More specifically, TY1, TY2, TY3, TY5 and TY7 with a vertical interval of 20 mm (1 m in prototype) were adopted to measure induced vertical earth pressure change. Horizontal or radial earth pressure was monitored by TY9, TY10 and TY11 with a horizontal separation of 20 mm (1 m in prototype). Similarly, multiple earth pressure sensors were installed to monitor earth pressure change induced by a model anchor in clay. Fig. 4(b) illustrates the instrumentation and monitoring plan. In total, 24 earth pressure sensors arranged in four arrays (A1-A4) were installed with various radii, i.e., 40, 80, 120 and 160 mm (equivalent to 2.8, 5.6, 8.4 and 11.2 m in prototype, respectively), from the anchor landing point. Each array consisted of 6 earth pressure sensors with an equal vertical spacing of 40 mm (i.e., 2.8 m in prototype). Each array of earth pressure sensors was attached to an aluminum rod before inserting into the prepared clay layer, and the monitoring data were transmitted to a data logger via wires. Note that TY earth pressure sensors manufactured by China Academy of Engineering Physics were used in this study, and the sensors were capable of measuring earth pressure change up to 500 kPa. In addition, a laser displacement

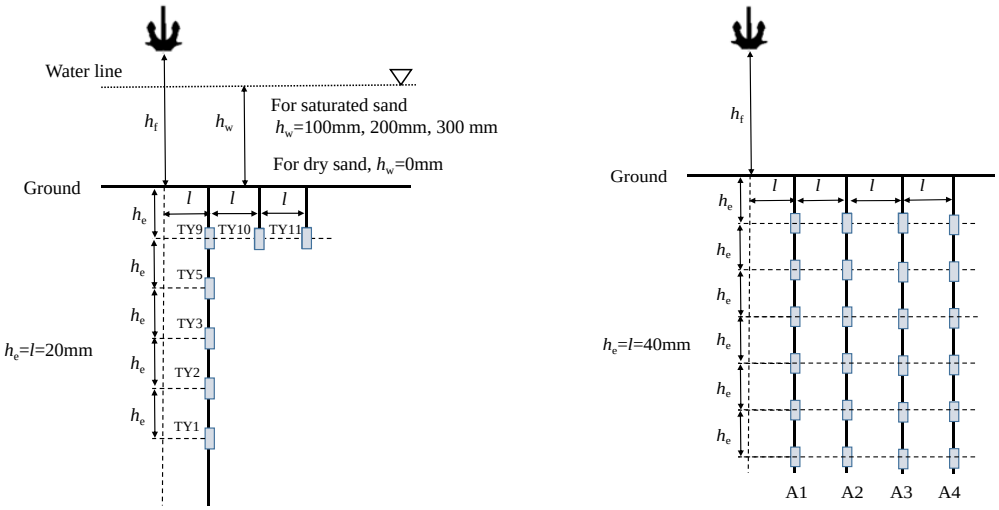

(a) sand (b) clay

Fig. 4 Instrumentation and monitoring plan

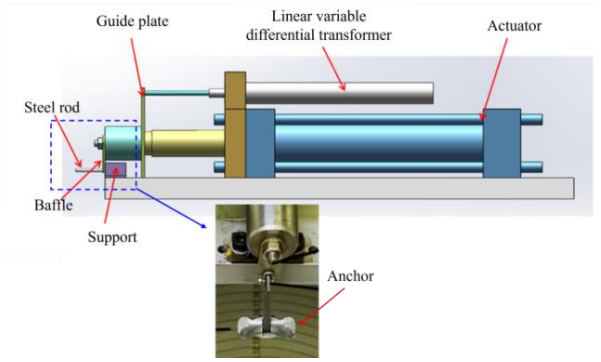

Fig. 5 Schematic diagram of anchor drop apparatus

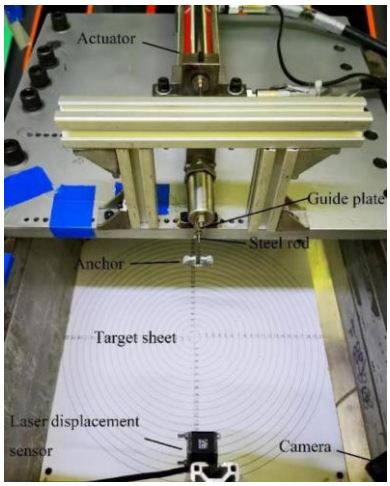

Fig. 6 Model setup

sensor is arranged near the landing point to verify the accurate anchoring height. In order to meet the accurate measurement in the process of anchor falling, the sampling frequency is set as 1000 Hz.

2.3 Anchor drop apparatus

A special designed apparatus was adopted to drop the model anchor during in-flight testing. Fig. 5 shows schematic diagram of the anchor drop apparatus. The actuator was adopted to push the anchor. Anchor hanged on the steel rod via baffle at a steady rate, which was considered slow enough to avoid the introduction of additional horizontal velocity to the model anchor during dropping operation. The horizontal displacement was measured by a linear variable differential transformer (LVDT), the sampling frequency is set as 1000Hz. It should be noted that the diameter of the steel rod was 2.5 mm, which was considered stiff enough to avoid excessive deformation induced by anchor when subjected to a centrifugal acceleration of 50 g and 70 g. In fact, the steel rod could be regarded as a cantilever beam subjected to a concentration force. Separate static mechanical analysis using Solidworks revealed that a maximum deflection of 0.14 mm could be induced when the anchor moved to the end of the steel rod.

2.4 Soil properties and model preparation

Two groups of centrifuge model tests were carried out in this study. The first group consisted of ten model tests in Toyoura sand, which is a uniform quartz sand that does not contain fines. The physical and mechanical properties of Toyoura sand were measured according to Chinese Stand for Soil Test Method (GB/T50123 2019). The sand has a mean diameter of 0.17 mm, a maximum void ratio of e_{max}=0.98, a minimum void ratio of e_{min}=0.60, a specific gravity of G_s=2.65, and an internal friction angle of φ'=30° at the critical state. The second group of model tests was conducted in saturated kaolin clay, which had a liquid limit of 61%, a plastic limit of 27%, G_s=2.6 and φ'=22°.

The first series of model tests was prepared using air pluvial deposition method. Initially, sand was rained from a hopper at a constant height over the sand surface in the strong box (Fretti *et al.* 1995, Hariprasad *et al.* 2016). The height was determined based on a target sand relative density (D_r) of 65%. For tests in saturated sand, water was supplied from the bottom drainage pipes until the water head reaching the designated water level. Subsequently, the

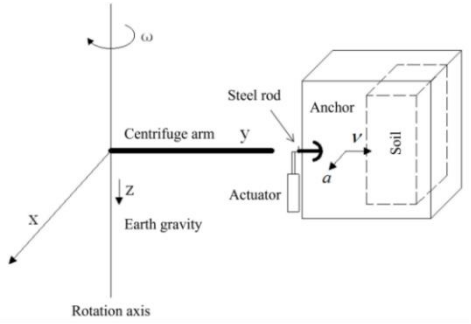

Fig. 7 Schematic diagram of the anchor drop system during spinning

anchor drop system was mounted on an alluvium plate, which was connected with the strong box (see Fig. 6). The whole dropping process was monitored and videoed.

The second series of model tests was prepared by mixing kaolin clay powder with water at about twice the liquid limit of the clay under a vacuum. Prior to pouring the clay slurry into a strong box for 1 g consolidation, a sand lay was placed at the bottom of the box followed by covering a filter paper to prevent mixing of sand and clay. More detailed engineering properties of the kaolin clay are referred to Stewart (1992), Bolton and Powrie (1987) and Ng and Wong (2013a). One-dimensional consolidation was carried out using a dead weight of 91 kPa, which was applied in stages to avoid overstressing. T-bar test was performed upon the end of 1 g consolidation to ensure that the undrained shear strength was around 20 kPa. In addition, clay samples were retrieved for laboratory testing and the unit weight was around 17 kN/m^3.

2.5 Testing procedure

After model preparation and a final check, the centrifuge was spun up to 50 g or 70 g in stages. The actuator was activated to push the model anchor at a slow rate until the anchor left the steel rod and dropped towards the sand bed. Fig. 7 shows the schematic diagram of the anchor drop system during centrifuge modelling.

3. Interpretation of centrifuge test results

All the results presented hereafter are converted to prototype scales according to the scaling laws listed in Table 1 unless stated otherwise. Fig. 8(a) shows the snapshot immediately before dropping the anchor, and Fig. 8(b) shows the moment when the dropped anchor reached the water surface. As effects of dropped anchors on submarine pipelines are closely related to the landing position, it is of great importance to investigate the relationships between the landing position and anchor drop height and associated water conditions.

3.1 Results of centrifuge model tests in sand

3.1.1 Coriolis effect on final land position of dropped anchor

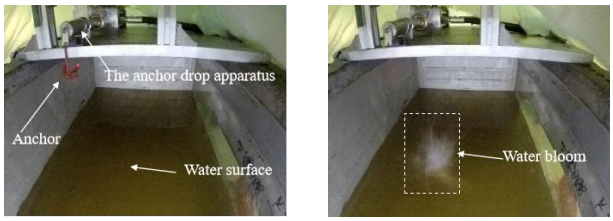

(a) Before anchor drop (b) After anchor drop

Fig. 8 Snapshots of anchor drop test in saturated sand

In centrifuge model test, the anchor was subjected to Coriolis effect (Chikatamarla 2009, Tomooka 2016), and the Coriolis acceleration can be estimated using the following equation

$$\vec{a}_c = 2v \times \vec{\omega} \tag{1}$$

where: $\vec{v}$ and $\vec{\omega}$ denote the dropping and the angular velocities, respectively. As shown in Fig. 9, the anchor moves along *y* direction once dropped from the steel rod, which is perpendicular to the angular velocity induced by clockwise rotation of the centrifuge arm. Following the cross-product operation in Eq. (1), the Coriolis acceleration points to the *x* direction. As a result, the anchor can drift towards the *x* direction. Assume the centrifugal acceleration is *ng* along *y* direction, and corresponding initial dropping velocity is zero. The horizontal offset, *s*, along *x* direction can be calculated as follows.

$$a_c = 2\omega v \tag{2}$$

$$v = ngt \tag{3}$$

$$h_d = \frac{1}{2} ngt^2 \tag{4}$$

$$s = \iint a_c dtdt = \frac{1}{3}\omega ngt^3 = \frac{2\omega}{3}\sqrt{\frac{2h_d^{\,3}}{ng}} \tag{5}$$

where *v* is the calculated dropping velocity along *y* direction and *t* is the total travel time for the dropped anchor reaching the sand bed; *h* is the total drop height of the anchor. In addition, the centrifugal acceleration, *ng*, can be evaluated as follows.

$$ng = \omega^2 r \tag{6}$$

The horizontal offset is rearranged as follows after substituting Eq. (6) into Eq. (5)

$$s = \frac{2}{3}\sqrt{\frac{2h_d^{\,3}}{r}} \tag{7}$$

where *r* represents the distance between the anchor and the rotation axis of the centrifuge and is taken as 3.8 m in this study. It can be seen from Eq. (7) that the horizontal offset is only related to the drop height of the anchor. The theoretical horizontal offsets for a set of drop heights are calculated and summarized in Table 4.

3.1.2 Effect of drop height and water depth on anchor offset

To facilitate the measurement of horizontal anchor

Table 4 Summary of calculated horizontal drift along x direction

Drop height (m)	10	15	20	25
Drift (m)	2.165	3.925	6.12	8.55

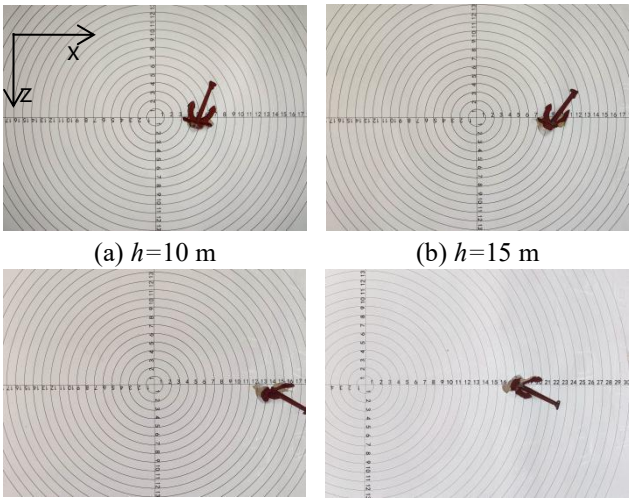

(a) h=10 m (b) h=15 m

(c) h=20 m (d) h=25 m

Fig. 9 Measured offset of a dropped anchor in dry sand

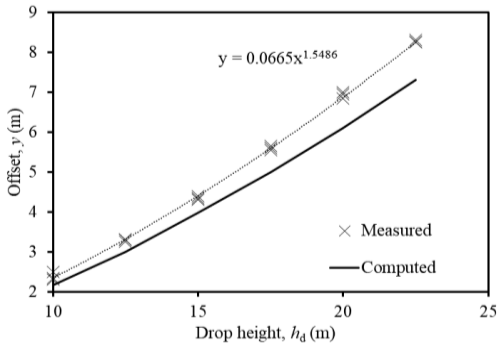

Fig. 10 Variation of offset with anchor drop height in dry sand

offset, a paper target sheet was placed on the surface of the sand bed. Fig. 9 shows the measured offset of the anchor in dry sand. As a result of Coriolis acceleration, the horizontal offset along x direction increased at an increased rate when the drop height elevated from 10 m to 25 m. At the same time, a horizontal offset of about 0.5 m was also measured along z direction as a result of the 1g earth gravitational acceleration. Note that the offset along z direction was much smaller than that along x direction because the Coriolis acceleration was much larger than the gravitational acceleration.

Fig. 10 shows a comparison of computed and measured horizontal offsets. It can be seen that three parallel experiments gave similar results and the computed horizontal offset had the same trend with the measured offset but with a relatively smaller magnitude. This can be explained by the fact that air resistance is not taken into consideration during theoretical derivation. The horizontal offset y can be expressed as an exponential function, as shown in Eq. (8).

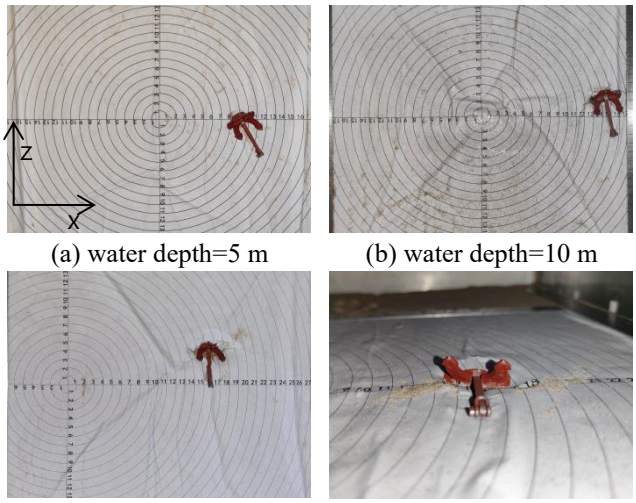

(a) water depth=5 m (b) water depth=10 m

(c) water depth=15 m

Fig. 11 Measured horizontal offset in saturated sand at different water levels

$$y = Ch_d^D \tag{8}$$

Where C and D are dimensionless coefficients. For the test results, C and D were 0.0665 and 1.5486, respectively.

Fig. 11 shows the measured horizontal offset in saturated sand. The water level varied between 5 m and 15 m, and the drop height of the anchor was fixed at 10 m above the designated water level. It can be seen that the horizontal offset was similar if the total drop height of the anchor above the sand bed was the same. For example, the measured offsets in Figs. 11(a), 13(b) and 11(c) were slightly smaller than those in Figs. 9(b), 9(c) and 9(d) due to the presence of water. In comparison, the offset caused by the earth gravity in the z direction exhibited an increasing trend with an increase in water depth. This can be explained by the fact that the velocity of the anchor significantly slowed down by the water. The deeper the water depth was, the longer the time required for reaching the sand bed became, resulting in an increase in the induced offset along earth gravity direction, i.e., z direction.

3.1.3 Temporal variation of anchor drop process

The travel time for the dropped anchor reaching the sand bed could be deduced from measurements of the laser displacement sensor or the earth pressure sensors embedded in the sand layer. Fig. 12 shows the relationship between measured travel time and the drop height. The theoretical values calculated from Eq. (4) have also been superimposed as a solid black line for comparison. It can be seen that the measured trends were generally in consistent with the theoretical calculations irrespective of water conditions. The measurements of the anchor drop tests in both dry and saturated sand exhibited a relatively large dispersion, which may possibly be caused by measurement errors. It is also noted that most measurements are larger than the computed values because air resistance slows down the dropping velocity of the anchor. In addition, the presence of water significantly increases the travel time as water can better decelerate the dropping velocity.

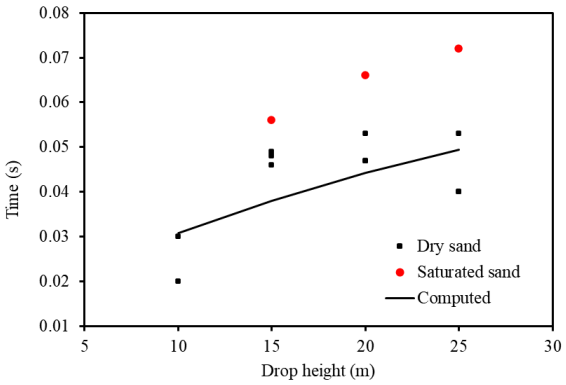

Fig. 12 Variation of measured travel time with anchor drop height

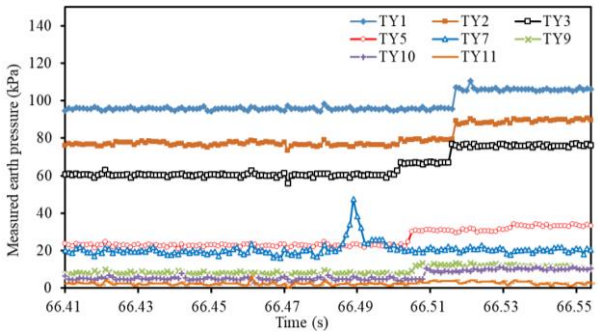

Fig. 13 Temporal variation of measured earth pressure with a drop height of 25 m in dry sand

3.1.4 Induced variation in earth pressure by dropped anchor

Due to page limit, only results from test nos. 7 and 10 are reported here. Fig. 13 shows the temporal variation of measured earth pressure at a drop height of 25 m in dry sand. It can be seen that the earth pressure measured by TY7 immediately increased from 20 kPa to 47 kPa in 0.003 s at a travel time of 64.484 s, followed by a rapid reduction to 22 kPa. In comparison, all the other earth pressure sensors started to respond after a time interval of 66.498 s, which indicates that it requires time for the propagation of earth pressure in sand. It is also observed that the measured earth pressures at shallow embedment depths (i.e., TY5 and TY7) exhibited an increasing trend followed by a gradual reduction.

In comparison, earth pressure sensors at deeper embedment depths recorded a monotonic increase, which implies that the influence depth of the impact force exerted by the dropped anchor was more than 5 m. The pressures measured by the other three sensors (i.e., TY9, TY10 and TY11) in the horizontal direction were much smaller than those in the vertical direction and decayed with an increase in horizontal distance. The change in earth pressure was negligible at the location of TY11, implying the horizontal influence zone was less than 3 m (equivalent to 12% of the dropped height).

Fig. 14 shows the temporal variation of measured earth pressure in saturated sand. The water depth was 15 m and the drop height of the anchor was 10 m above the water level. The initial response was recorded by TY7. The

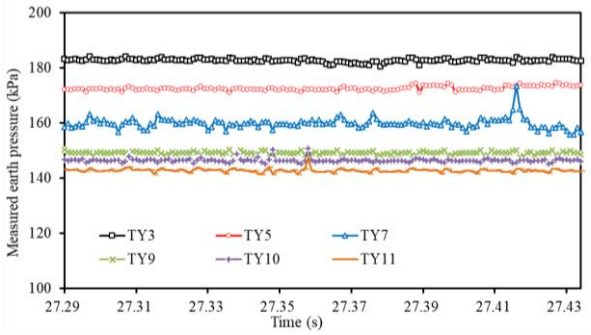

Fig. 14 Temporal variation of measured earth pressure with a water depth of 15 m and a drop height of 10 m above water level in saturated sand

measured earth pressure rose quickly to a peak of about 170 kPa followed by a rapid reduction to its initial value. In comparison, the earth pressure increased by 2 kPa at the location of TY5, i.e., 2 m below the sand bed. Other sensors with deeper embedments remained almost unchanged, which implies that the maximum influence depth was less than 3 m. In addition, TY9 in the horizontal direction recorded a temporal stress increment of 5 kPa, which subsequently disappeared. No significant stress change was observed by TY10 and TY11 and the influence zone in the horizontal direction was less than 2m.

It is worthwhile to compare the measured earth pressure in Figs. 13 and 14. It is found that the deeper the water level is, the smaller the influence zone caused by the dropped anchor is. It implies that water is effective in decelerating the anchor and reducing the kinematic energy imposed on the sand bed. It is also noted that some sensors observe a reduction in measured earth pressure once the anchor landed on the sand bed. This can be explained by the fact that the submerged density of the saturated sand is less than the density of dry sand and the imposed impact force tends to change the locations of those sensors.

3.1.5 Analytical solution for calculating influence depth of dropped anchor

Mindlin solution is used to solve the stress and strain in an elastic semi-infinite space subjected to a concentration force (Selvadurai *et al*. 1993, 2016). In this study, the influence zone caused by the impact force of a dropped anchor was back-calculated based on the measured earth pressures as follows.

$$\sigma_k = \frac{F}{s^2} I_p \tag{9}$$

where I_p can be expressed as follows.

$$\begin{aligned} I_p = \frac{1}{8\pi(1-\mu)} \Bigg\{ & \frac{(1-2\mu)(m-1)}{A^3} \\ & - \frac{(1-2\mu)(m-1)}{B^3} + \frac{3(m-1)^3}{A^5} \\ & + \frac{3(3-4\mu)m(m+1)^2 - 3(m+1)(5m-1)}{B^5} \\ & + \frac{30m(m+1)^3}{B^7} \Bigg\} \end{aligned} \tag{10}$$

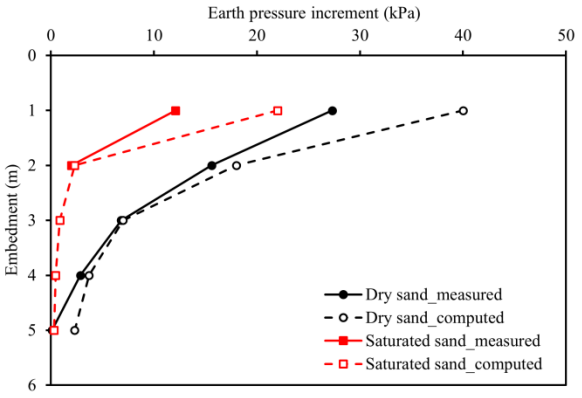

Fig. 15 Comparison of measured and computed earth pressure

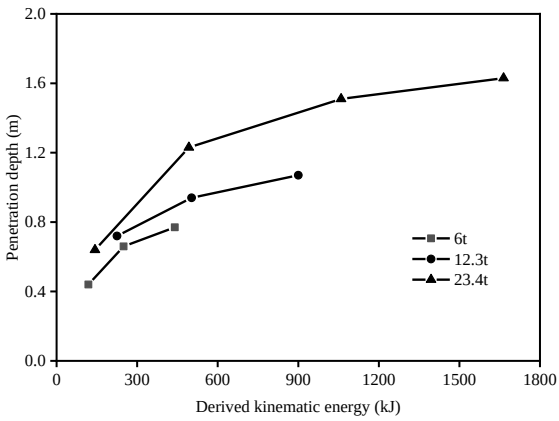

Fig. 16 Relationship of penetration depth with kinematic energy

where $A = \sqrt{n^2 + (m-1)}$

$B = \sqrt{n^2 + (m+1)}$

$n = r/s$

$m = z/s$

where μ is Possion's ratio; r denotes the radial distance between a calculation point and the landing point of the dropped anchor; z is the depth between a calculation point and the dropped anchor; s represents the penetration depth of the anchor.

Fig. 15 shows the comparison of measured and computed earth pressures along depth. Essentially, the computed earth pressure profiles shared the similar trend with the measured profiles but with a relatively larger magnitude. This can be explained by the fact that plastic zones were generated during the penetration process of the anchor, thus Mindlin solution, assuming elastic field, can overestimate the induced earth pressure. In addition, there was an increasing trend in sand stiffness with depth, which is also different from the constant stiffness used for derivation of Eq. (9). It is also observed that the difference

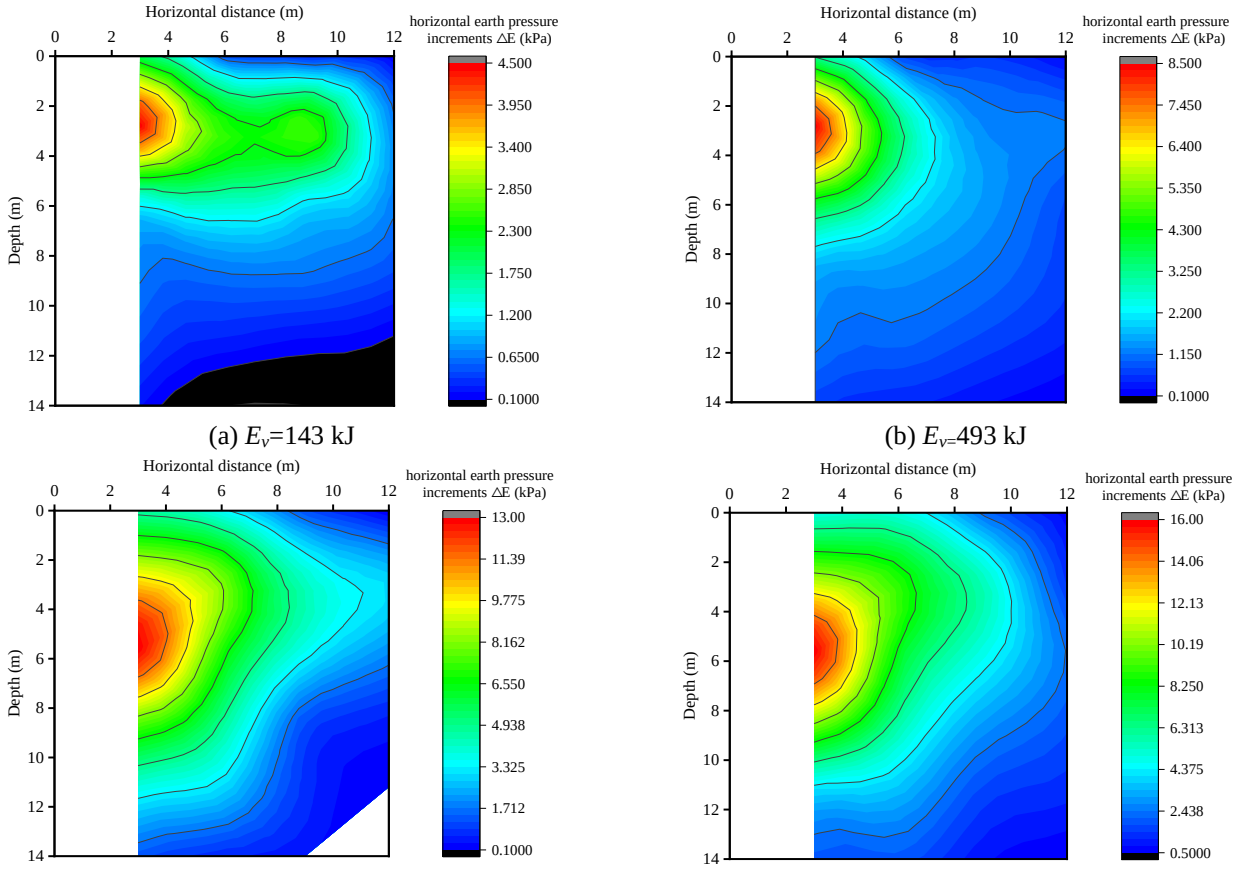

(a) E_v=143 kJ (b) E_v=493 kJ

(c) E_v=1060 kJ (d) E_v=1665 kJ

Fig. 17 Contour of horizontal earth pressure change

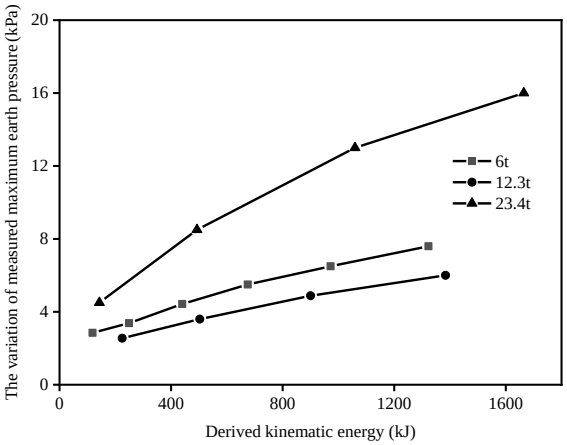

Fig. 18 Relationship between maximum earth pressure change and kinematic energy

between the computed and measured earth pressures enlarged at areas closer to the anchor. This can possibly because the sensors had relatively low sampling frequency, which could fail to capture the peak pressure caused by the instantaneous impact force.

3.2 Results of centrifuge model tests in clay

3.2.1 Penetration depth of drop anchor

Fig. 16 shows the relationship of measured penetration depth of drop anchor with derived kinematic energy. As mentioned in subsection 3.1.1, the gravitational potential energy of a drop anchor can be converted to kinematic energy through a theoretical relationship. As expected, there is an increasing trend of penetration depth with kinematic energy. For example, the measured penetration depth of a 6 ton drop anchor is about 0.4 m at a drop height of approximately 2 m (i.e., 118.5 kJ). The penetration depth significantly increases by 50% and 87.5% and reaches 0.6m and 0.75 m when the kinematic energy increases to 250 kJ and 440 kJ, respectively. Similar results are observed for the tests using a 12.3 ton drop anchor. The penetration depth grows steadily from 0.75 m to approximate 1.0 m when the kinematic energy increases from 224.9 kJ (i.e., a drop height of 1.9 m) to 900.3 kJ (equivalent to a drop height of 7.5 m). For the test using a 23.4 ton drop anchor, there is a rapid increase in the penetration depth when the kinematic energy is less than 500 kJ. Afterwards, the penetration depth increases steadily with the kinematic energy but at a reducing rate. It is also worth pointing out that a heavier anchor is shown to result in a larger penetration depth at the same given kinematic energy. For example. When the kinematic energy equals 500 kJ, the penetration depths induced by the 23.4 ton and 12.3 ton anchor are 54% and 31% larger than that of a 6 ton anchor. The difference may possibly be attributed to the way how the kinematic energy is calculated. The value of kinematic energy, as shown in Fig. 18, only considers the effects of centrifugal acceleration and does not take the gravitational and Coriolis acceleration into consideration. As demonstrated in Figs. 11 and 13, the Coriolis acceleration may have a significant effect on the performance of a drop anchor.

3.2.2 Variation of induced earth pressure

Fig. 17 shows the contour of horizontal earth pressure increments (ΔE) subjected to a 23.4 ton drop anchor with different maximum kinematic energy (E_v). To avoid excessive disturbances, sensors were only installed at 2.8 m away from the landing point of a dropped anchor. Fig. 17(a) shows the contour of measured earth pressure increment at E_v=143 kJ. Note that ΔE varies between 0 and 4.5 kPa, and the maximum locates at about 3 m below the ground surface, which is slightly deeper that the final penetration depth of 0.6 m at E_v=143 kJ (see Fig. 16) is about 0.6 m. There is a gradual reduction in the recorded earth pressure change when the distance increases along both horizontal and vertical directions. Not that the deduced contour is oval, implying the decay of earth pressure increment is faster in the vertical direction than that in the horizontal direction. The measured earth pressure change is negligible at a horizontal distance of about 12 m. In comparison, when E_v increases to 493 kJ, the earth pressure contour becomes more circular and there is concurrent downward shift in the depth of maximum ΔE. It is also observed that the depth of maximum ΔE keeps increasing to about 5 m and 6 m when E_v increases to 1060 kJ and 1665 kJ (equivalent to a drop height of 4.6 m and 7.3 m), respectively. At the same time, the recorded maximum ΔE increases by 189% and 256% as compared with that at E_v=143 kJ. This is attributed to the fact that larger soil strains are induced in order to dissipate the large imposed kinematic energy. It is also worth pointing out that all the measured results are applicable to the kaolin clay with an undrained shear strength of 20 kPa. In order to reduce the effects of a drop anchor, one possible solution is to increase the strength of seabed materials.

To improve the understanding of relationship between earth pressure increment and kinematic energy, the variation of measured maximum earth pressure (ΔE_{max}) is plotted against kinematic energy in Fig. 18. It can be seen that similar non-linear patterns are observed irrespective of weights of anchors. The measured ΔE_{max} is about 4 kPa when the kinematic energy is equal to or less than 900 kJ for both the 6 ton and 12.3 ton anchors. In comparison, ΔE_{max} induced by the 23.4 ton anchor increases dramatically from about 4.5 kPa to approximately 16 kPa at the final kinematic energy of 1665 kJ.

4. Conclusions

In this study, a series of centrifuge model tests was conducted to investigate penetration mechanisms of a A-type Hall anchor subjected to different drop heights and water depths. Based on the current study, the following conclusions may be drawn:

- Results indicate that Coriolis acceleration was the governing factor determining the horizontal offset during centrifuge model test. In comparison, earth gravity had negligible effect on the displacement of the dropped anchor. The horizontal offset and anchor drop height can be expressed by exponential function. It is also found the measured horizontal displacement caused by Coriolis effect shared a similar trend with measurements in dry sand but with a relatively smaller

magnitude, which was mainly attributed to the existence of air resistance. In addition, the existence of ground water further reduced the horizontal movement of the anchor, resulting in a reduction in measured horizontal offset. The offset along the earth gravity direction also increased as the time required for the dropped anchor reaching the sand bed increased due to the resistance of water in saturated sand.

• The influence zone of the impact force caused by a dropped anchor is closely related to the water conditions and drop height. At a drop height of 25 m in dry sand, the vertical influence depth and horizontal influence radius were larger than 5 m and 3 m, respectively. With a water level of 5 m, a drop height of 10 m above the water level could result in a vertical influence depth and a horizontal influence radius of smaller than 3 m and 2 m, respectively, implying that the influence zone is significantly affected by the water conditions. As an increase in water depth, the impact force exerted by a dropped anchor decreased, resulting in a diminished effect on the potential submarine structures.

• For model tests in clay, there was a continuous increase in the recorded penetration depth with kinematic energy. The maximum penetration depth was around 1.6 m for a 23.4 ton anchor with a kinematic energy value of 1665 kJ. The induced maximum earth pressure change lay slightly below the maximum penetration depth of each anchor. The contour of earth pressure increment for a 23.4 ton anchor initially had an oval shape at low kinematic energy (i.e., 143 kJ) and became circular at larger kinematic energy values. It is also found that there was a non-linear increasing trend between recorded maximum earth pressure increment with kinematic energy.

• The Minglin solution can well reflect the nonlinear characteristics of the additional earth pressure weakening with depth. The earth pressure increment calculated by the Mindelin solution due to anchor penetration is in good agreement with the measured value. The additional stress caused by anchor penetration of submarine pipeline can be calculated by using the Minglin solution.

Acknowledgements

The authors would like to acknowledge the financial support provided by the Fundamental Research Funds (Nos. TKS20200309 and TKS190203) for the Central Public Welfare Research Institutes and grant 51809132 of NSFC of China.

References

Abdollahi, M. and Bazaz, J.B. (2017), "Reconstitution of sand specimens using a rainer system", *Int. J. Eng.*, **37**(3), 1451-1463. https://doi.org/10.5829/ije.2017.30.10a.05.

Bolton, M.D. and Powrie, W. (1987), "The collapse of diaphragm walls retaining clay", *Geotechnique*, **37**(3), 335-353. https://doi.org/10.1680/geot.1987.37.3.335.

Chikatamarla, R., Laue, J. and Springman, S.M. (2006), "Centrifuge scaling laws for guided free fall events including rockfalls", *Int. J. Phys. Model. Geotech.*, **6**(2), 15-26. http://doi.org/10.1016/S09333630(96)00135-3.

Cho, H.I., Sun, C.G., Kim, J.H. and Kim, D.S. (2018), "OCR evaluation of cohesionless soil in centrifuge model using shear wave velocity", *Geomech. Eng.*, **15**(4), 987-995. https://doi.org/10.12989/gae.2018.15.4.987.

Craig, W.H., James, R.G. and Schofield, A.N. (1988), *Centrifuges in Soil Mechanics*, Crc Press.

Fang, J.C., Kong, G.Q. and Yang, Q. (2022), "Group performance of energy piles under cyclic and variable thermal loading", *J. Geotech. Geoenviron. Eng.*, **148**(8), 04022060. https://doi.org/10.1061/(ASCE)GT.1943-5606.0002840.

Fretti, C., Presti, D.C.F.L. and Pedroni, S. (1995), "A pluvial deposition method to reconstitute well-graded sand specimens", *Geotech. Test. J.*, **18**(2), 292-298. https://doi.org/10.1520/GTJ10330J.

Gao. Q., Duan M.L., Liu, X.H., Wang, Y., Jia, X., An, C. and Zhang, T. (2018), "Damage assessment for submarine photoelectric composite cable under anchor impact-science direct", *Appl. Ocean Res.*, **73**, 42-58. https://doi.org/10.1016/j.apor.2018.01.006.

General Administration of Quality Supervision, Inspection and Quarantine of the People's Republic of China and Standardization Administration of the People's Republic of China (2016), Hall Anchor, (GB/T546-2016), Beijing, China. (in Chinese)

Han, C.C., Chen, X.J. and Liu, J. (2019), "Physical and numerical modeling of dynamic penetration of ship anchor in clay", *J. Waterw. Port Coast. Ocean Eng.*, **145**(1), 04018030. https://doi.org/10.1061/(ASCE)WW.1943-5460.0000490.

Hariprasad, C., Rajashekhar, M. and Umashankar, B. (2016), "Preparation of uniform sand specimens using stationary pluviation and vibratory methods", *Geotech. Geolog. Eng.*, **34**(6), 1909-1922. https://doi.org/10.1007/s10706-016-0064-0.

Hu, K., Zhang, C.H., Zhou, R.Z. and Gao, F. (2021), "A research for the safety influence of dropping anchor on the submarine pipeline", *IOP Conf. Ser. Earth Environ. Sci.*, **621**, 012075. https://doi.org/10.1088/1755-1315/621/1/012075.

Liu, R., Wang, J.Y. and Bie, S.A. (2020), "Study of the penetration depth of an anchor in the dropping anchor process", *J. Tianjin Univ. (Sci. Technol.)*, **53**(5), 508-516. https://doi.org/cnki:sun:tjdx.0.2020-05-009. (in Chinese)

Madabhushi, G. (2015), *Centrifuge Modelling for Civil Engineers*, CRC Press/Taylor & Francis.

Ministry of Housing and Urban Rural Development of the People's Republic of China and State Administration for Market Regulation (2019), Standard for geotechnical testing method (GB/T 50123-2019), Beijing, China. (In Chinese)

Nakamura, M., Nanayakkara, N., Hatazaki, H. and Tsuji, K. (2002), "Reliability analysis of submarine power cables and determination of external mechanical protections", *IEEE Trans. Power Deliv.*, **7**(2), 895-902. https://doi.org/10.1109/61.127096.

Ng, C.W.W. and Wong, K.S. (2013a), "Investigation of passive failure and deformation mechanisms due to tunnelling in clay", *Can. Geotech. J.*, **50**(4), 359-372. https://doi.org/10.1139/cgj-2012-0098.

Ng, C.W.W., Shi, J.W. and Hong, Y. (2013b), "Three-dimensional centrifuge modelling of basement excavation effects on an existing tunnel in dry sand", *Can. Geotech. J.*, **50**(8), 874-888. . https://doi.org/10.1139/cgj-2012-0423.

Ouyang, Y., Zhang, L., Gan, L., Zheng, Y. and Wang, Z. (2016), "Research on numerical simulation of submarine pipeline impacted by an anchor", *The 26th International Ocean and Polar Engineering Conference*, OnePetro.

Selvadurai, A.P.S. (1993), "The axial loading of a rigid circular

anchor plate embedded in an elastic half-space", *Int. J. Numer. Anal. Meth. Geomech.*, **17**(5), 343-353. https://doi.org/10.1002/nag.1610170505.

Selvadurai, A.P.S. and Katebi, A. (2016), "The boussinesq-mindlin problem for a non-homogeneous elastic halfspace", *Zeitschrift für angewandte Mathematik und Physik*, **67**(3), 1-15. https://doi.org/10.1007/s00033-016-0661-z.

Shi, J.W., Chen Y.H., Lu, H., Ma, S.K. and Ng, C.W.W. (2022a), "Centrifuge modeling of the influence of joint stiffness on pipeline response to underneath tunnel excavation", *Can. Geotech. J.*, **59**(9), 1568-1586. https://doi.org/10.1139/cgj-2020-0360.

Shi, J.W., Wei, J.Q., Ng, C.W.W., Lu, H. Ma, S.K., Shi, C. and Li P. (2022b), "Effects of construction sequence of double basement excavations on an existing floating pile", *Tunnel. Underg. Space Technol.*, **119**, 104230. https://doi.org/10.1016/j.tust.2021.104230.

Shin, H.K., Seo, B.C. and Lee, J.H. (2011), "Experimental study of embedding motion and holding power of drag embedment type anchor (dea) on sand seafloor", *Int. J. Nav Arch. Ocean Eng.*, **3**(3), 193-200. https://doi.org/10.3744/jnaoe.2011.3.3.193.

Stewart, D.P. (1992), "Lateral loading of piled bridge abutments due to embankment construction", Ph.D. Thesis, The University of Western Australia, Perth.

Taylor, R.N. (1995), *Geotechnical Centrifuge Technology*, CRC Press.

Tian, Y., Chai, W., Borgi, S.E., Zhang, C. and Fu, D. (2021), "Assessment of submarine pipeline damages subjected to falling object impact considering the effect of seabed", *Marine Struct.*, **78**(5), 102963. https://doi.org/10.1016/j.marstruc.2021.102963.

Tomooka, R., Itoh, K., Tanaka, T. and Suemasa, N. (2019), "Reproduction of slope failure due to rainfall in a centrifuge model test", *KEC Conference 2019*, Kantipur Engineering College, Dhapakhel Lalitpur.

True, D.G. (1975), "Penetration of projectiles into seafloor soils", True Civil Engineering Laboratory (Navy) Port Hueneme, California, USA.

Wang, C., Zhou, S., Wang, B. and Guo, P. (2018), "Time effect of pile-soil-geogrid-cushion interaction of rigid pile composite foundations under high-speed railway embankments", *Geomech. Eng.*, **16**(6), 589-597. https://doi.org/10.12989/gae.2018.16.6.589.

Wang, L.Q., Chia, H.K., Wei, J.W. and Chen, Q. (2009), "FEA-based study of pipeline protection from anchors", *ASME 2009 28th International Conference on Ocean, Offshore and Arctic Engineering*, Hawaii, USA.

Wang, W., Wang, X. and Yu, G. (2016), "Penetration depth of torpedo anchor in cohesive soil by free fall", *Ocean Eng.*, **116**, 286-294. https://doi.org/10.1016/j.oceaneng.2016.03.003.

Zhang, H., Zhang, J., Lin, R. and Li, Y. (2020), "Numerical study on mechanism responses of submarine pipeline impacted by bar-shaped falling object", *J. Pipeline Syst. Eng. Pract.*, **11**(4), 04020051. https://doi.org/10.1061/(ASCE)PS.1949-1204.0000505.

Zhu, X., Hao, Q. and Zhang, J. (2019), "Buried depth of a submarine pipeline based on anchor penetration", *J. Marine Sci. Eng.*, **7**(8), 257. https://doi.org/10.3390/jmse7080257.